# Energy and enstrophy spectra and fluxes for the inertial-dissipation range of two-dimensional turbulence

Akanksha Gupta,[1,*] Rohith Jayaram,[2] Anando G. Chaterjee,[1] Shubhadeep Sadhukhan,[1] Ravi Samtaney,[3] and Mahendra K. Verma[1,†]

[1]*Department of Physics, Indian Institute of Technology, Kanpur 208016, India*

[2]*Department of Energy and Process Engineering, Norwegian University of Science and Technology, Trondheim NO-7491, Norway*

[3]*Mechanical Engineering, Division of Physical Science and Engineering, King Abdullah University of Science and Technology, Thuwal 23955-6900, Kingdom of Saudi Arabia*

(Received 10 April 2019; revised manuscript received 7 August 2019; published 4 November 2019)

In this paper, using Pao's conjecture [Y.-H. Pao, Phys. Fluids **8**, 1063 (1965)], we derive expressions for the spectra and fluxes of kinetic energy and enstrophy for two-dimensional (2D) forced turbulence that extend beyond the inertial range. In these expressions, the fluxes and the spectra contain additional factors of the exponential form. To validate these model predictions, we perform numerical simulations of 2D turbulence with external force applied at wavenumber band $(k_f, k_f + 1)$ in the intermediate range. The numerical results match with the model predictions, except for the energy and enstrophy fluxes for $k < k_f$, where the fluxes exhibit significant fluctuations. We show that these fluctuations arise due to the unsteady nature of the flow at small wavenumbers. For $k < k_f$, the shell-to-shell energy transfers computed using numerical data show forward energy transfers among the neighboring shells, but backward energy transfers among other shells.

DOI: 10.1103/PhysRevE.100.053101

## I. INTRODUCTION

Turbulence is an omnipresent phenomenon [1–5]. Though many natural and laboratory flows are three dimensional, many astrophysical and geophysical flows exhibit two-dimensional (2D) or quasi-two-dimensional behavior [6–11]. For example, strong rotation suppresses the velocity component in the direction of rotation [12–14]. Similarly, a strong external magnetic field in magnetohydrodynamics [15–18] and strong gravity in planetary environments [19–21] make the flow quasi-two-dimensional. Therefore, a good understanding of 2D turbulence is important for modeling such flows. In this paper, we address the spectra and fluxes of energy and enstrophy for the inertial-dissipation range of 2D turbulence.

Using analytical arguments, Kraichnan [22] predicted a dual cascade for 2D turbulence that is forced at an intermediate scale ($k \approx k_f$). He showed an inverse cascade of kinetic energy for $k < k_f$, and forward cascade of enstrophy for $k > k_f$. In the corresponding regimes, the kinetic energy spectra are $E_u(k) = C\epsilon^{2/3}k^{-5/3}$ and $E_u(k) = C'\epsilon_\omega^{2/3}k^{-3}$, respectively; here $\epsilon$ and $\epsilon_\omega$ are respectively the energy and enstrophy dissipation rates (or injection rates), and $C$ and $C'$ are constants. Using numerical simulations, Paret and Tabeling [23] computed $C$ and observed it to be approximately $C \approx 6.5 \pm 1$. For $k > k_f$, numerical simulations of Gotoh [24] predict that $C'$ varies from 0.596 to 0.931 when the simulation grid is increased from $1024^2$ to $4096^2$. Lindborg and Vallgren [19] observed that $C' \simeq 1.3$. Using field-theoretic tools, Nandy and Bhattacharjee [25] derived that $C \simeq 6.447$ and $C' \simeq 1.923$. Furthermore, Kraichnan [26] derived a logarithmic correction to the latter spectrum. Using the properties of structure function, Gotoh [24] generalized the spectrum of the forward enstrophy cascade regime to the dissipation range. He argued that $E_u(k) \propto k^{-(3+\delta)}$ for $k < k_{d2D}$, and $E_u(k) \propto k^{-(3+\delta)/2}\exp(-\alpha_2 k/k_{d2D})$ for $k > k_{d2D}$, where $k_{d2D} = \epsilon_\omega^{1/6}/\sqrt{\nu}$ is the enstrophy dissipation wavenumber, and $\delta$ and $\alpha_2$ are constants. Gotoh [24] also verified the above scaling using numerical simulation.

Kraichnan's formulas for the dual energy spectrum have been observed in many laboratory experiments, for example, by Paret and Tabeling [23], Rutgers [27], and Kellay *et al.* [28]. In numerical simulations, the same phenomena have also been observed by Siggia and Aref [29], Frisch and Sulem [30], and Borue [31]. For a forced 2D turbulence, the large-scale energy grows in time [32]. In the regime with forward enstrophy transfer, the energy spectrum is typically steeper than $k^{-3}$, both in numerical simulations [33] and in experiments [34]. Moreover, Scott [35]and Fontane *et al.* [36] reported some deviations from the theoretical predictions of Kraichnan [22]. Pandit *et al.* [37] described properties of 2D flows in the presence of complex forces. Eghdami *et al.* [38] studied the energy transfer between the synoptic scale and the mesoscale using direct numerical simulation (DNS) of 2D turbulence under forcing applied at different scales.

Boffetta [39] performed direct numerical simulations of forced 2D Navier-Stokes equations and studied the energy and enstrophy cascade regimes with good accuracy. Boffetta [39] also employed Ekman friction to suppress energy growth at large scales. Besides the above spectral laws, variable energy flux and irregular and nonlocal energy transfer have also been studied for 2D turbulence [40]. Musacchio and Boffetta

*akgupt@iitk.ac.in

†mkv@iitk.ac.in

 

[41] investigated the formation of large-scale structures in a turbulent fluid confined in a thin layer. However, despite many years of work, there are some discrepancies on the scaling laws. Also, see Ref. [5] for a description of various properties of energy fluxes, including those of 2D turbulence.

Kolmogorov's theory [42,43] yields a $k^{-5/3}$ energy spectrum for three-dimensional (3D) hydrodynamic turbulence. Pao [44,45] generalized this scaling to the inertial-dissipation range by postulating that the ratio of the energy spectrum and energy flux is independent of kinematic viscosity, and that it depends on the dissipation rate and local wavenumber. We employ Pao's conjecture [45] to 2D turbulence, and extend the $k^{-5/3}$ and $k^{-3}$ spectra and corresponding fluxes [22] beyond the inertial range.

In this paper we report our results on the numerical study of forced 2D turbulence. In forced 2D turbulence, to suppress the growth of kinetic energy at large scales, it is customary to either introduce Ekman friction (as in Ref. [39]) or fine-tune the small wavenumber modes (as in Ref. [36]). However, a flip side of the above schemes is that they affect the inertial range dynamics. One of the objectives of our present study is to investigate the locality of energy transfers in the $k < k_f$ regime via shell-to-shell energy transfers and energy flux. For the same, it is important not to suppress the effects of the nonlinear term, $\mathbf{u} \cdot \nabla \mathbf{u}$, by an additional dissipation like Ekman friction. For this reason, we avoided the usage of Ekman friction or removal of large-scale energy. In addition, in our study we also compute the spectra and fluxes of energy and enstrophy, and compare the numerical results with the predictions of the extended model of Pao [44]. For $k > k_f$, we observe good agreement between the numerical results and model predictions. However, model predictions and numerical results differ for the $k < k_f$ regime, possibly due to the unsteady nature of 2D turbulence.

The present paper is structured as follows. In Sec. II, we describe the governing equations for a forced two-dimensional incompressible fluid. In Sec. III we derive the spectra and fluxes of energy and enstrophy using Pao's conjecture. In Sec. IV, we describe our numerical procedure and parameter values. Section V contains simulation results and comparison with model predictions. We conclude in Sec. VI.

## II. GOVERNING EQUATIONS

The Navier-Stokes equations for a forced two-dimensional incompressible fluid are

$$\frac{\partial \mathbf{u}}{\partial t} + \mathbf{u} \cdot \nabla \mathbf{u} = -\nabla p + \nu \nabla^2 \mathbf{u} + \mathbf{F}_u, \tag{1}$$

$$\nabla \cdot \mathbf{u} = 0, \tag{2}$$

where $\mathbf{u}$ and $p$ are the velocity and pressure fields, respectively, $\nu$ is the kinematic viscosity, and $\mathbf{F}_u$ is the external force. We take density to be constant ($\rho = 1$). The flow is two dimensional in the $xy$ plane, and the vorticity is a scalar: $\omega = (\nabla \times \mathbf{u}) \cdot \hat{z}$. Taking a curl of Eq. (1) yields the following dynamical equation for the vorticity field:

$$\frac{\partial \omega}{\partial t} + \mathbf{u} \cdot \nabla \omega = \nu \nabla^2 \omega + F_\omega, \tag{3}$$

where $F_\omega = [\nabla \times \mathbf{F}_u]_z$.

For a 2D hydrodynamic flow, the total kinetic energy (KE), $E_u$, and the total enstrophy, $E_\omega$, are defined below:

$$E_u = \int d\mathbf{r} u^2(\mathbf{r})/2, \quad E_\omega = \int d\mathbf{r} \omega^2(\mathbf{r})/2. \tag{4}$$

These quantities are conserved for 2D flows in the inviscid and force-free regime [1–4]. These quadratic invariants play an important role in 2D turbulence.

The above equations for the velocity and vorticity fields are written in Fourier space as

$$\frac{d}{dt}\mathbf{u}(\mathbf{k}) + \mathbf{N}_u(\mathbf{k}) = -i\mathbf{k}p(\mathbf{k}) + \mathbf{F}_u(\mathbf{k}) - \nu k^2 \mathbf{u}(\mathbf{k}), \tag{5}$$

$$\frac{d}{dt}\omega(\mathbf{k}) + N_\omega(\mathbf{k}) = F_\omega(\mathbf{k}) - \nu k^2 \omega(\mathbf{k}), \tag{6}$$

$$\mathbf{k} \cdot \mathbf{u}(\mathbf{k}) = 0, \tag{7}$$

where

$$\mathbf{N}_u(\mathbf{k}) = i \sum_{\mathbf{p}} \{\mathbf{k} \cdot \mathbf{u}(\mathbf{q})\}\mathbf{u}(\mathbf{p}), \tag{8}$$

$$N_\omega(\mathbf{k}) = i \sum_{\mathbf{p}} \{\mathbf{k} \cdot \mathbf{u}(\mathbf{q})\}\omega(\mathbf{p}), \tag{9}$$

with $\mathbf{q} = \mathbf{k} - \mathbf{p}$. Note that the pressure $p(\mathbf{k})$ is derived by taking the dot product of Eq. (5) with $i\mathbf{k}$ and by employing $\mathbf{k} \cdot \mathbf{u}(\mathbf{k}) = 0$:

$$p(\mathbf{k}) = \frac{i}{k^2}\mathbf{k} \cdot \{\mathbf{N}_u(\mathbf{k}) - \mathbf{F}_u(\mathbf{k})\}. \tag{10}$$

To derive a dynamical equation for the modal KE $E_u(\mathbf{k}) = |\mathbf{u}(\mathbf{k})|^2/2$ and modal enstrophy $E_\omega(\mathbf{k}) = |\omega(\mathbf{k})|^2/2$, we perform dot products of Eq. (5) with $\mathbf{u}^*(\mathbf{k})$, and of Eq. (6) with $\omega^*(\mathbf{k})$, and add the resultant equations with their complex conjugates. These operations yield

$$\begin{aligned}\frac{\partial}{\partial t}E_u(\mathbf{k}) &= \sum_{\mathbf{p}} \mathrm{Im}[\{\mathbf{k} \cdot \mathbf{u}(\mathbf{q})\}\{\mathbf{u}(\mathbf{p}) \cdot \mathbf{u}^*(\mathbf{k})\}] \\ &\quad + \mathrm{Re}[\mathbf{F}_u(\mathbf{k}) \cdot \mathbf{u}^*(\mathbf{k})] - 2\nu k^2 E_u(\mathbf{k}) \\ &= T_u(\mathbf{k}) + \mathcal{F}_u(\mathbf{k}) - D_u(\mathbf{k})\end{aligned} \tag{11}$$

and

$$\begin{aligned}\frac{\partial}{\partial t}E_\omega(\mathbf{k}) &= \sum_{\mathbf{p}} \mathrm{Im}[\{\mathbf{k} \cdot \mathbf{u}(\mathbf{q})\}\{\omega(\mathbf{p})\omega^*(\mathbf{k})\}] \\ &\quad + \mathrm{Re}[F_\omega(\mathbf{k})\omega^*(\mathbf{k})]) - 2\nu k^2 E_\omega(\mathbf{k}) \\ &= T_\omega(\mathbf{k}) + \mathcal{F}_\omega(\mathbf{k}) - D_\omega(\mathbf{k}),\end{aligned} \tag{12}$$

where Re[·], Im[·] are real and imaginary parts of the argument, respectively; $T_u(\mathbf{k})$ and $T_\omega(\mathbf{k})$ are respectively the rate of KE and enstrophy transfers to the modal KE and modal enstrophy by nonlinearity; $\mathcal{F}_u(\mathbf{k})$ and $\mathcal{F}_\omega(\mathbf{k})$ are respectively the modal KE and enstrophy injection rates by the external force; and $D_u(\mathbf{k})$ and $D_\omega(\mathbf{k})$ are respectively the dissipation rates of the modal KE and enstrophy. We define

KE and enstrophy fluxes for a wavenumber sphere of radius $k_0$ as

$$\Pi_u(k_0) = -\int_0^{k_0} T_u(k)dk, \tag{13}$$

$$\Pi_\omega(k_0) = -\int_0^{k_0} T_\omega(k)dk. \tag{14}$$

Using the above equations we can derive the following equations for one-dimensional spectra [4,21]:

$$\frac{\partial}{\partial t}E_u(k,t) = -\frac{\partial}{\partial k}\Pi_u(k,t) + \mathcal{F}_u(k,t) - D_u(k,t), \tag{15}$$

$$\frac{\partial}{\partial t}E_\omega(k,t) = -\frac{\partial}{\partial k}\Pi_\omega(k,t) + \mathcal{F}_\omega(k,t) - D_\omega(k,t). \tag{16}$$

In the next section we employ the above equations to derive spectra and fluxes for the KE and enstrophy in the inertial range and beyond.

## III. THE SPECTRA AND FLUXES OF KINETIC ENERGY AND ENSTROPHY BEYOND THE INERTIAL RANGE

In this section we extend Kraichnan's [22] formulas for the KE and enstrophy spectra and fluxes beyond the inertial range using Pao's conjecture [44]. For three-dimensional hydrodynamic turbulence, there are several models for the inertial-dissipation ranges. They are by Pao [44], Pope [46], and Martínez *et al.* [47]. Among these models, one by Pao provides the best fit to the numerical data, as demonstrated by Verma *et al.* [48]. In addition, Pao's model has no additional parameter.

Motivated by these successes, we attempted Pao's conjecture to model two-dimensional turbulence that has two regimes: $k < k_f$ and $k > k_f$. Fortunately, the model predictions fit reasonably well with the numerical data in the inertial-dissipation range. In the literature it has been a challenge to model the $k > k_f$ range, but, as we demonstrate in the paper, Pao's model works quite well for this regime.

Under a steady state, in Eqs. (15) and (16), we set $\partial/\partial t = 0$. In addition, in the inertial range, the injection rates by the external force vanish, while the dissipation rates are negligible. Hence,

$$\frac{d}{dk}\Pi_u(k) = 0, \quad \frac{d}{dk}\Pi_\omega(k) = 0, \tag{17}$$

which leads to constancy of KE and enstrophy fluxes. Kraichnan [22] showed that $\Pi_u(k)$ is constant for $k < k_f$, while $\Pi_\omega(k)$ is constant for $k > k_f$. For these regimes, dimensional analysis yields [22]

$$E_u(k) = C\bar{\Pi}_u^{2/3}k^{-5/3} \quad \text{for } k < k_f, \tag{18}$$

$$E_u(k) = C'\bar{\Pi}_\omega^{2/3}k^{-3} \quad \text{for } k > k_f, \tag{19}$$

where $\bar{\Pi}_u$ and $\bar{\Pi}_\omega$ are respectively the values of the KE and enstrophy fluxes in the inertial range, and $C$ and $C'$ are constants. In Sec. V we show that $\bar{\Pi}_u$ and $\bar{\Pi}_\omega$ differ from $\epsilon$ and $\epsilon_\omega$, respectively. In this paper we take the maximum value of the respective fluxes for $\bar{\Pi}_u$ and $\bar{\Pi}_\omega$.

To extend the above scaling beyond the inertial range, but still away from the forcing range, we retain $D_u(k)$ and $D_\omega(k)$ in Eq. (17) which yields

$$\frac{d}{dk}\Pi_u(k) = -2\nu k^2 E_u(k), \tag{20}$$

$$\frac{d}{dk}\Pi_\omega(k) = -2\nu k^2 E_\omega(k). \tag{21}$$

The above relations are valid for all wavenumbers. The above two equations have four unknowns; hence they cannot be uniquely solved. To overcome this difficulty, we extend Pao's conjecture [45] for 3D hydrodynamic turbulence to 2D turbulence which enables us to extend the energy and enstrophy spectra beyond the inertial range. In the following two sections we describe them for $k < k_f$ and $k > k_f$ regimes separately.

### A. $k < k_f$

We assume that for $k < k_f$, $E_u(k)/\Pi_u(k)$ is a function of $\bar{\Pi}_u$ and $k$, and it is independent of $\nu$ and the forcing parameters. Under these assumptions, dimensional analysis yields

$$\frac{E_u(k)}{\Pi_u(k)} = -C\bar{\Pi}_u^{-1/3}k^{-5/3}. \tag{22}$$

Note that the negative sign in Eq. (22) is due to the fact that $\Pi_u(k) < 0$. Substitution of Eq. (22) in Eq. (20) yields

$$\frac{d}{dk}\Pi_u(k) = 2C\nu\bar{\Pi}_u^{-1/3}k^{1/3}\Pi_u(k), \tag{23}$$

whose solution is

$$\Pi_u(k) = -\bar{\Pi}_u \exp\left(\tfrac{3}{2}C(k/k_d)^{4/3}\right), \tag{24}$$

$$E_u(k) = C\bar{\Pi}_u^{2/3}k^{-5/3}\exp\left(\tfrac{3}{2}C(k/k_d)^{4/3}\right), \tag{25}$$

where $k_d = (\bar{\Pi}_u/\nu^3)^{1/4}$ and $\bar{\Pi}_u > 0$.

Now we investigate enstrophy flux in this regime. It is generally conjectured that $\Pi_\omega(k) \approx 0$ in this regime [11,39]. But this is not the case because Eqs. (20) and (21) yield

$$\frac{d\Pi_\omega(k)}{d\Pi_u(k)} = k^2. \tag{26}$$

In fact, we can determine the enstrophy flux using Eq. (21) in the following manner. Substitution of $E_u(k)$ of Eq. (25) in Eq. (21) yields

$$\begin{aligned}\Pi_\omega(k) &= -2\nu\int^k k'^4 E_u(k')dk' \\ &= -2\nu C\bar{\Pi}_u^{2/3}\int^k k'^{7/3}\exp\left(\frac{3}{2}C(k'/k_d)^{4/3}\right)dk' \\ &= -2\nu C\bar{\Pi}_u^{2/3}k_d^{10/3}\int^x dx' x'^{7/3}\exp\left(\frac{3}{2}Cx'^{4/3}\right),\end{aligned} \tag{27}$$

where $x' = k'/k_d$.

In the following section we describe the energy flux and spectrum, as well as enstrophy flux in the $k > k_f$ regime.

### B. $k > k_f$

In this regime we assume that $E_\omega(k)/\Pi_\omega(k)$ is a function of $\bar{\Pi}_\omega$ and $k$, and it is independent of $\nu$ and forcing function. This assumption leads to

$$\frac{E_\omega(k)}{\Pi_\omega(k)} = C'\bar{\Pi}_\omega^{-1/3}k^{-1}. \tag{28}$$

Substitution of Eq. (28) in Eq. (21) yields

$$\frac{d}{dk}\Pi_\omega(k) = -2C'\nu\bar{\Pi}_\omega^{-1/3}k\Pi_\omega(k), \tag{29}$$

whose solution is

$$\Pi_\omega(k) = \bar{\Pi}_\omega \exp\left(-C'(k/k_{d2D})^2\right), \tag{30}$$

$$E_\omega(k) = C'\bar{\Pi}_\omega^{2/3}k^{-1}\exp\left(-C'(k/k_{d2D})^2\right), \tag{31}$$

$$E_u(k) = C'\bar{\Pi}_\omega^{2/3}k^{-3}\exp\left(-C'(k/k_{d2D})^2\right), \tag{32}$$

where $k_{d2D} = \bar{\Pi}_\omega^{1/6}/\sqrt{\nu}$ is the enstrophy dissipation wavenumber. Note that $E_u(k)$ of Eq. (32) is steeper than $k^{-3}$ in the inertial-dissipation range. The strong Gaussian factor dominates $k^{-3}$ scaling; this could be the reason for the difficulty in observing the $k^{-3}$ spectrum in the $k > k_f$ regime. In Sec. V we show consistency of the above steepening with the numerical results.

To determine $\Pi_u(k)$, we substitute $E_u(k)$ of Eq. (32) in Eq. (20), and integrate the equation from $k$ to $\infty$. Using $\Pi_u(\infty) = 0$ and making a change of variable $x = C'(k/k_{d2D})^2$, we obtain

$$\begin{aligned}\Pi_u(k) &= 2\nu\int_k^\infty k'^2E_u(k')dk' \\ &= \frac{\bar{\Pi}_\omega C'}{k_{d2D}^2}\int_x^\infty \frac{1}{x'}\exp(-x')dx' \\ &= \frac{\bar{\Pi}_\omega C'}{k_{d2D}^2}E_1(C'(k/k_{d2D})^2),\end{aligned} \tag{33}$$

where $E_1$ is the exponential integral [49].

Since $k_{d2D}$ represents the enstrophy dissipation wavenumber, $k_f/k_{d2D} < k/k_{d2D} \lessapprox 1$. In this range, $E_1(x)$ is of the order of unity. For example, $E_1(x) < 2$ for $0.1 < x < 1.6$ [49]. Hence,

$$\Pi_u(k) \approx \frac{\bar{\Pi}_\omega C'}{k_{d2D}^2} \tag{34}$$

and $\Pi_u$ and $\Pi_\omega$ have different units. But, in nondimensional form, $k_{d2D}$ is of the order of $k_{\max}$ or $N/2$, where $N$ is the grid size. Therefore, using Eq. (34) we deduce that in nondimensional units, $\Pi_u(k) \ll \bar{\Pi}_\omega$ in the forward enstrophy regime. This observation is consistent with the findings of Gotoh [24] that $\Pi_u(k) \to 0$ in the inertial-dissipation range ($k > k_f$). However, the functional form of $\Pi_u(k)$ in Ref. [24] differs from that of Eq. (33).

Note, however, that the aforementioned expressions of spectra and fluxes of KE and enstrophy assume steady state. As we show in Sec. V, in the absence of Ekman friction, this assumption holds only approximately due to the unsteady nature of 2D turbulence. As a result, some of the above predictions match with the simulation results, while some do not.

We attempt to verify the above scaling functions using numerical simulations.

## IV. DETAILS OF NUMERICAL SIMULATIONS

In the present paper, we perform numerical simulations of forced 2D hydrodynamic turbulence using the spectral method. The system is doubly periodic in a domain of size $2\pi \times 2\pi$. We employ two different grid resolutions, $2048^2$ and $8192^2$, to make sure that our results are grid independent. The equations are solved using the fully dealiased, parallel pseudospectral code TARANG [50,51] with a fourth-order Runge-Kutta time-marching scheme. For dealiasing purposes, a 2/3 rule is chosen [52,53]. The viscosity for the $2048^2$ and $8192^2$ grids are set at $10^{-3}$ and $3 \times 10^{-4}$, respectively, which yields corresponding Reynolds numbers of $1.2 \times 10^4$ and $4.2 \times 10^5$. For our simulation we employ eddy turnover time as a unit of time. We run our simulations for the two grids up to $t_{\text{final}} = 10.0$ and 1.74, respectively. We employ a Courant-Friedrichs-Lewy (CFL) condition to determine the time step $dt$. For the two grids, the average time steps are $3.4 \times 10^{-5}$ and $6.9 \times 10^{-5}$, respectively.

We force the flow at wavenumber bands $k_f = (50, 51)$ and (100, 101) for $2048^2$ and $8192^2$ grids, respectively. For both these simulations, the energy supply rates are 20 nondimensional units. These resolutions provide more than a decade of inverse cascade regime. The enstrophy cascades forward in the $k > k_f$ regime, but the spectrum is steeper than $k^{-3}$ due to the dissipation effects. Using the numerical data we compute the one-dimensional energy and enstrophy spectra using

$$E_u(k) = \frac{1}{2}\sum_{k-1<|\mathbf{k}'|\leqslant k}|\mathbf{u}(\mathbf{k}')|^2, \tag{35}$$

$$E_\omega(k) = \frac{1}{2}\sum_{k-1<|\mathbf{k}'|\leqslant k}|\omega(\mathbf{k}')|^2. \tag{36}$$

For the above forcing, we obtain an approximate steady state, as illustrated in Fig. 1 where we plot the total energy vs time for both the grids, as well as $E_u(k)$ vs $k$ for the $8192^2$ grid. We obtain an approximate steady state even without Ekman friction because $E_u(k)$ is significantly large at small $k$ leading to considerable viscous dissipation in the wavenumber band $(0, k_f)$, as illustrated in Table I. This is due to the large initial kinetic energy (∼200) compared to some of the earlier 2D simulations reported in the literature. Note that the total dissipation rates differ by approximately 20% from the energy injection rates (20), possibly due to the unsteady nature of 2D turbulence. Complex dynamics arising due to the forcing at the intermediate range may also play a role in these discrepancies.

In this paper we report the energy and enstrophy fluxes. The energy flux $\Pi_u(k_0)$ is defined as the energy leaving the sphere of radius $k_0$ due to nonlinearity. This quantity is computed as [54,55]

$$\Pi_u(k_0) = \sum_{|\mathbf{p}|\leqslant k_0}\sum_{|\mathbf{k}|>k_0} S^{uu}(\mathbf{k}|\mathbf{p}|\mathbf{q}), \tag{37}$$

TABLE I. Total and partial viscous dissipation rates (columns 2 and 3) and total and partial enstrophy dissipation (columns 5 and 6). Here, $\mathcal{M}(|\Pi_u(k<k_f)|)$ and $\mathcal{M}(|\Pi_\omega(k>k_f)|)$ represent $\max(|\Pi_u(k<k_f)|)$ and $\max(|\Pi_\omega(k>k_f)|)$, respectively.

| Data type | $2\nu\int_0^{k_{\max}} k'^2 E_u(k')dk'$ | $2\nu\int_0^{k_f} k'^2 E_u(k')dk'$ | $\mathcal{M}(\lvert\Pi_u(k<k_f)\rvert)$ | $2\nu\int_0^{k_{\max}} k'^4 E_u(k')dk'$ | $2\nu\int_{k_f}^{k_{\max}} k'^4 E_u(k')dk'$ | $\mathcal{M}(\lvert\Pi_\omega(\mathrm{k}>\mathrm{k_f})\rvert)$ |
|---|---|---|---|---|---|---|
| Single time frame data of $2048^2$ grids | 24.0 | 16.4 | 16.1 | $5.54\times10^4$ | $3.64\times10^4$ | $3.24\times10^3$ |
| Single time frame data of $8192^2$ grids | 24.5 | 21.7 | 81.3 | $1.26\times10^5$ | $5.00\times10^4$ | $1.64\times10^4$ |
| Time-averaged data of $2048^2$ grids | 24.7 | 16.0 | 4.73 | $7.15\times10^4$ | $4.80\times10^4$ | $4.00\times10^3$ |
| Time-averaged data of $8192^2$ grids | 25.8 | 20.7 | 38.1 | $2.23\times10^5$ | $1.41\times10^5$ | $6.45\times10^4$ |

where

$$S^{uu}(\mathbf{k}|\mathbf{p}|\mathbf{q}) = \mathrm{Im}[\{\mathbf{k}\cdot\mathbf{u}(\mathbf{q})\}\{\mathbf{u}(\mathbf{p})\cdot\mathbf{u}^*(\mathbf{k})\}] \tag{38}$$

is the *mode-to-mode* energy transfer from Fourier mode $\mathbf{u}(\mathbf{p})$ to Fourier mode $\mathbf{u}(\mathbf{k})$ with Fourier mode $\mathbf{u}(\mathbf{q})$ acting as the mediator. Note that the wavenumbers $(\mathbf{k},\mathbf{p},\mathbf{q})$ form a triad with $\mathbf{k}=\mathbf{p}+\mathbf{q}$. Similarly, we compute the enstrophy flux as

$$\Pi_\omega(k_0) = \sum_{|\mathbf{p}|\leqslant k_0}\sum_{|\mathbf{k}|>k_0} S^{\omega\omega}(\mathbf{k}|\mathbf{p}|\mathbf{q}), \tag{39}$$

where

$$S^{\omega\omega}(\mathbf{k}|\mathbf{p}|\mathbf{q}) = \mathrm{Im}[\{\mathbf{k}\cdot\mathbf{u}(\mathbf{q})\}\{\omega(\mathbf{p})\omega^*(\mathbf{k})\}] \tag{40}$$

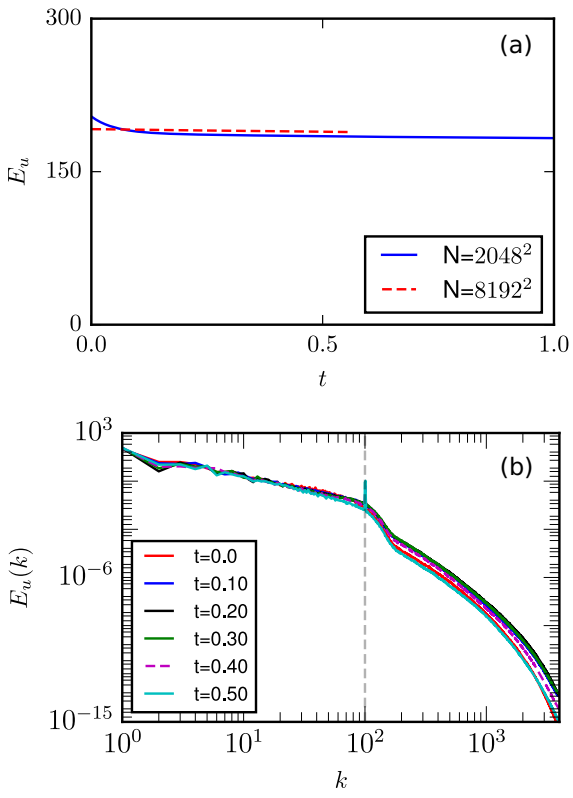


FIG. 1. (a) Plot of total energy $E$ vs $t$ for $2048^2$ grid (blue solid curve) and $8192^2$ grid (dashed red curve). (b) Plot of $E_u(k)$ vs $k$ at various times for the $8192^2$ grid simulation. These plots indicate approximate steady states for the simulation runs.

is the *mode-to-mode* enstrophy transfer from mode $\omega(\mathbf{p})$ to mode $\omega(\mathbf{k})$ with mode $\mathbf{u}(\mathbf{q})$ acting as the mediator.

The energy and enstrophy fluxes provide insights into the global transfers in the system. For a more detailed picture, we compute the shell-to-shell energy transfers. We divide the wavenumber space into various concentric shells. The shell-to-shell energy transfer from shell $m$ to shell $n$ is given by

$$T^{u,m}_{u,n} = \sum_{\mathbf{p}\in m}\sum_{\mathbf{k}\in n} S^{uu}(\mathbf{k}|\mathbf{p}|\mathbf{q}). \tag{41}$$

In the present work, we compute the shell-to-shell energy transfer for the $k<k_f$ regime. We compare our numerical result with those for 3D hydrodynamic turbulence for which the energy transfer is local and forward in the inertial range; that is, the dominant energy transfer is from shell $m$ to $m+1$. For better resolution, we perform the shell-to-shell transfer computations for the $8192^2$ grid with log-binned shells. We divide the Fourier space into 20 concentric shells; the inner and outer radii of the $i$th shell are $k_{i-1}$ and $k_i$, respectively. The shell radii for $N=8192^2$ grids are $k_i=\{0,2,4,8,8\times 2^{s(i-3)},\ldots,2048,4096\}$, where $s=8/15$ and $i$ is the shell index. Inertial range shells have been chosen by logarithmic binning because of the power-law physics in the inertial range.

In this paper we do not report the shell-to-shell enstrophy transfer in the $k>k_f$ regime due to a lack of constant enstrophy regime because of strong dissipation. In future we plan to perform simulations with $k_f\approx 1$ that would provide a significant wavenumber range of constant enstrophy flux. It will be meaningful to perform shell-to-shell enstrophy transfer computations using such data.

As we describe in the following section, the energy and enstrophy fluxes in the $k<k_f$ regime are highly fluctuating, possibly due to the unstable nature of 2D turbulence. Therefore, in addition to illustrating the above fluxes for single snapshots for $2048^2$ and $8192^2$ grids, we also present averages of these fluxes over 35 frames.

The formulas for the energy and enstrophy fluxes and spectra described in the previous section require values of $C$, $C'$, $\bar{\Pi}_u$, $\bar{\Pi}_\omega$, $k_d$, and $k_{d2D}$. Numerical simulations and analytical calculations [11,24,25,32] predict that $C\approx 6.5\pm 1$, and $C'\approx$ 1–2 (see Sec. I). In this paper we choose $C=6.5$ and $C'=1.0$, consistent with the above results. The estimation of the dissipation rates $\bar{\Pi}_u$ and $\bar{\Pi}_\omega$ for two-dimensional

TABLE II. Values of $k_d$ and $k_{d2D}$ for the four cases given in Table I.

| Data type | $k_d$ | $k_{d2D}$ |
|---|---|---|
| Single time frame data of $2048^2$ grids | $3.56 \times 10^2$ | $2.94 \times 10^2$ |
| Single time frame data of $8192^2$ grids | $1.32 \times 10^3$ | $6.82 \times 10^2$ |
| Time-averaged data of $2048^2$ grids | $2.62 \times 10^2$ | $3.15 \times 10^2$ |
| Time-averaged data of $8192^2$ grids | $1.09 \times 10^3$ | $8.20 \times 10^2$ |

turbulence is tricky. Since the flow is forced at an intermediate wavenumber band, we compute the energy and enstrophy dissipation rates in both $k < k_f$ and $k > k_f$ regimes and list them in Table I. As shown by the entries of the table, there are strong energy and enstrophy dissipation in the $k < k_f$ band, contrary to three-dimensional hydrodynamic turbulence, where dissipation occurs at large $k$'s. This is because of the large magnitude of $E_u(k)$ in this regime. Also, for the total dissipation rates, $\epsilon_\omega \approx k_f^2 \epsilon$, as expected. Interestingly, the dissipation rates do not match with the maximum values of the energy and enstrophy fluxes, which are denoted by $\mathcal{M}(|\Pi_u|)$ and $\mathcal{M}(|\Pi_\omega|)$, respectively. For the best fit to the numerical results of Sec. V, we take $\bar{\Pi}_u = \mathcal{M}(|\Pi_u(k < k_f)|)$ and $\bar{\Pi}_\omega = \mathcal{M}(|\Pi_\omega(k > k_f)|)$.

Lastly, we estimate $k_d = (\epsilon/\nu^3)^{1/4}$. However, the forward enstrophy cascade regime does not have a significant $k^{-3}$ power-law regime for the spectrum; hence we cannot use the formula $k_{d2D} = \epsilon_\omega^{1/6}/\sqrt{\nu}$ for its estimation. Rather, we obtain $k_{d2D}$ from the best fit curve to the enstrophy flux. These parameters are listed in Table II. We employ these parameters in Eqs. (24), (25), (30), (32), and (33) to compute the best fit curves for modeling the numerical results.

In the next section we report numerical results on the spectra and fluxes of energy and enstrophy.

## V. RESULTS AND DISCUSSIONS

In the present section we report the numerically computed spectra and fluxes of energy and enstrophy. We compare these results with the model predictions of Sec. III.

### A. Energy spectra

In this subsection, we describe the energy and enstrophy spectra of 2D turbulence. In Figs. 2(a) and 2(b) we plot these spectra for $2048^2$ and $8192^2$ grids. The numerically computed spectra are exhibited using red solid curves, and the model predictions of Sec. III using dashed black curves. In this figure we also plot the predictions of Kraichnan's theory using solid black lines.

For $k < k_f$, the numerical results and model predictions yield $E_u(k) \sim k^{-5/3}$, which is the prediction of Kraichnan [22]. For $k > k_f$, $E_u(k)$ is steeper than Kraichnan's [22] predictions of $k^{-3}$ [24,33,34]. The steepening of $E_u$ compared to $k^{-3}$ is due to the dissipative effects, more so because of the $\exp(-(k/k_{d2D})^2)$ factor. Model equation (32) overestimates the energy spectrum. This is possibly due to the lack of inertial range, and due to uncertainties in $k_{d2D}$. A more refined simulation is required to decipher this issue. Also, we compared our numerical results and predictions with those of Gotoh [24] in the limiting cases and observed general agreement. Note that $E_\omega(k) = k^2 E_u(k)$; hence $E_\omega(k)$ is not reported separately.

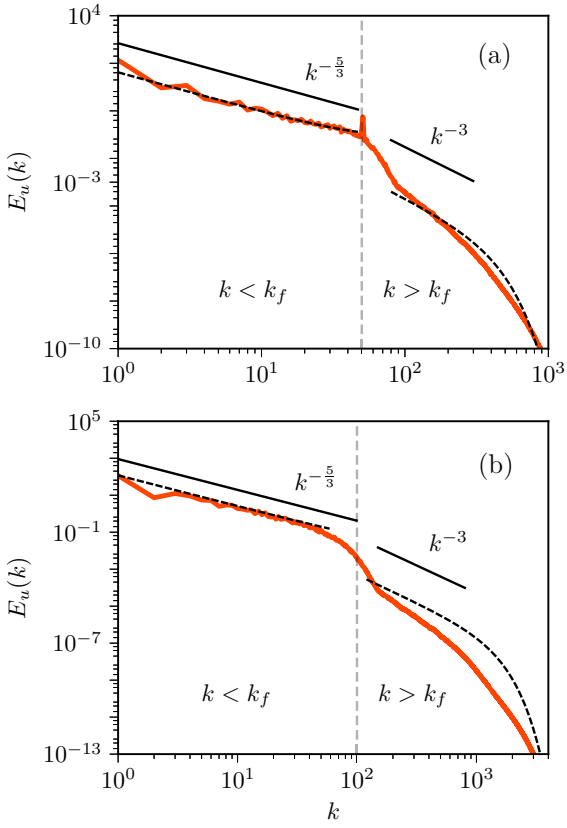


FIG. 2. Kinetic energy spectra for single time frames each of 2D forced turbulence on the (a) $2048^2$ grid and (b) $8192^2$ grid. The forcing wavenumbers are indicated by dashed vertical lines. The plots exhibit numerical results (solid red curves), model predictions [Eqs. (25) and (32)] (dashed black curves), and Kraichnan [22]'s predictions (solid black lines). The model predictions are in general agreement with numerical results. Fitting parameters are given in Tables I and II.

In the next subsection we describe the energy and enstrophy fluxes computed using the numerical data, as well as those predicted by the model of Sec. III.

### B. Energy and enstrophy fluxes

We compute the energy and enstrophy fluxes for 2D turbulence using Eqs. (37) and (39). We compute these quantities for both grid resolutions ($2048^2$ and $8192^2$). The numerically computed fluxes are exhibited in Fig. 3. The left- and right-hand panels of Fig. 3 illustrate the energy and enstrophy fluxes, respectively.

The top panel of Fig. 3 exhibits the energy and enstrophy fluxes for a single time frame of the $2048^2$ grid run. We observe that these fluxes exhibit significant fluctuations for $k < k_f$. Therefore, we compute average fluxes. The fluxes in the middle and bottom panels are computed by averaging over 35 different time frames for $2048^2$ and $8192^2$ grids, respectively. In the plots, the red curves represent the numerically computed fluxes, while the black dashed curves represent the model predictions of Sec. III.

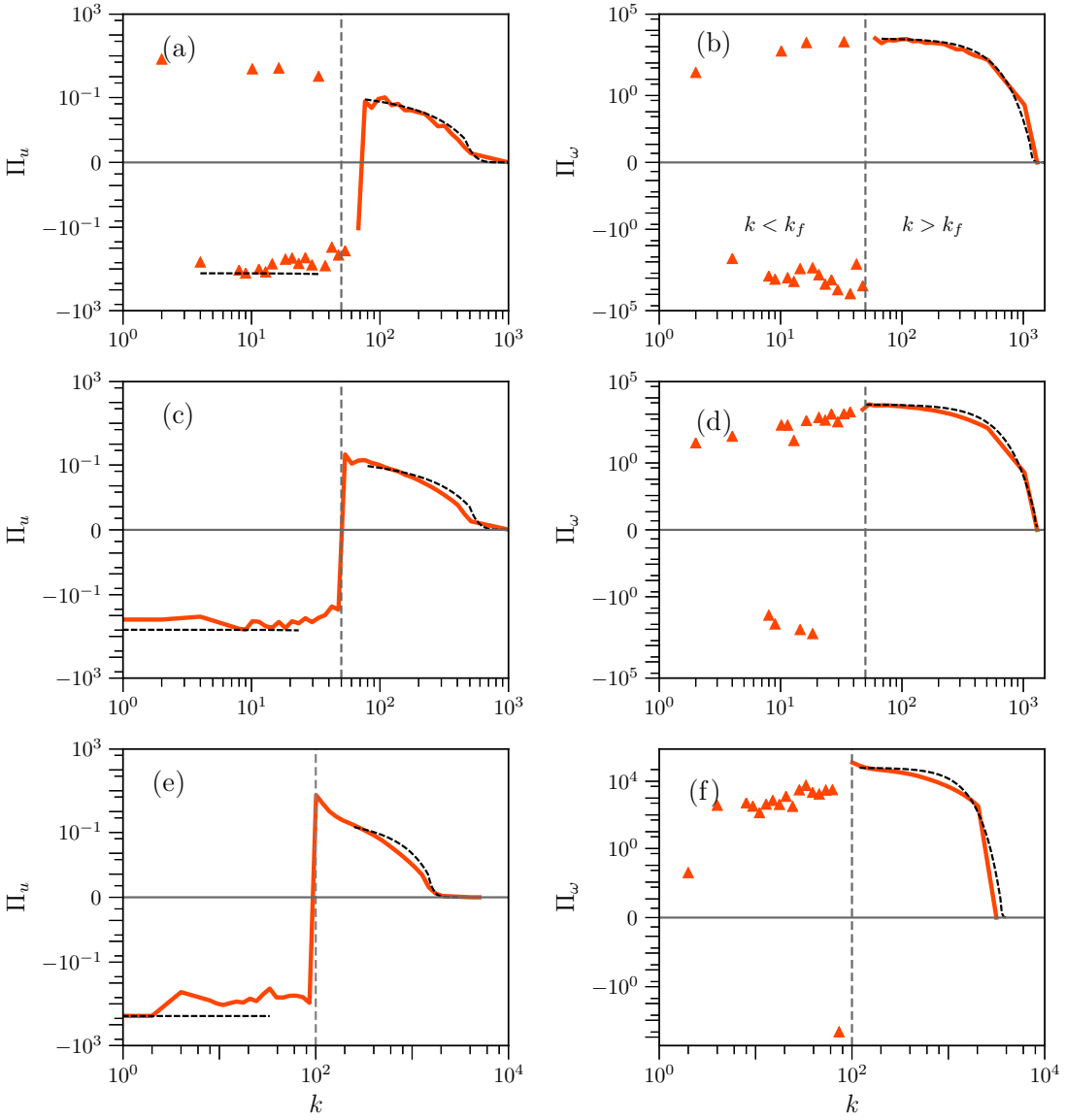


FIG. 3. Plots of kinetic energy flux, $\Pi_u(k)$ (left panel), and enstrophy fluxes, $\Pi_\omega(k)$ (right panel): (a, b) for a single time frame of $2048^2$ run, (c, d) time averaged $\Pi_u(k)$ and $\Pi_\omega(k)$ over 35 frames of the $2048^2$ run, and (e, f) time averaged $\Pi_u(k)$ and $\Pi_\omega(k)$ over 35 frames of the $8192^2$ run. The numerical results (red solid lines) match with the model predictions [Eqs. (30) and (33)] (black dashed lines) in the $k > k_f$ regime. The discrepancies in the $k < k_f$ regime are possibly due to the unsteady nature of the flow. Note that the plots are in log-log scale because of the huge range of scales of $\Pi_u(k)$ and $\Pi_\omega(k)$.

A careful observation of the figure shows that for $k > k_f$, the model predictions of the KE and enstrophy fluxes, Eqs. (30) and (33), are in good agreement with the numerical results. Thus, Eqs. (30) and (33) describe 2D turbulence satisfactorily for the $k > k_f$ regime. Note that in this regime, both $\Pi_u(k)$ and $\Pi_\omega(k)$ fall very sharply due to the Gaussian nature of the exponential factor $[\exp(-(k/k_{d2D})^2)]$. Also, $\Pi_u(k) \ll \Pi_\omega(k)$, consistent with Eq. (34) and the predictions of Gotoh [24]. This is somewhat surprising in that the model predictions overestimate the energy spectrum in this regime. This issue needs further investigation.

However, for $k < k_f$, the model predictions fail to describe the numerical results well. As shown in Figs. 3(a) and 3(b), the energy and enstrophy fluxes computed using the data from a single frame exhibit significant fluctuations. The fluctuations are somewhat suppressed on averaging, as shown in Figs. 3(c)–3(f), yet the enstrophy flux for the $8192^2$ grid shows large fluctuations in the $k < k_f$ regime. We believe that the fluctuations in the fluxes are due to the unsteady nature of the flow.

Two-dimensional turbulence exhibits an inverse cascade of kinetic energy that leads to the formation of large-scale structures. An imbalance between the viscous dissipation and the energy feed at the large-scale structures makes the flow unsteady. As a result, Eqs. (20) and (21) are not valid for the $k < k_f$ regime. To quantify the unsteadiness of the flow, we compute all the terms of Eq. (15) for the $2048^2$ grid and compare them. In Fig. 4 we plot $|\partial E(k)/\partial t|$ and $|-d\Pi_u(k)/dk - D_u(k)|$ with respect to $k$. Though the left-hand and right-hand sides of Eq. (15) match with each other,

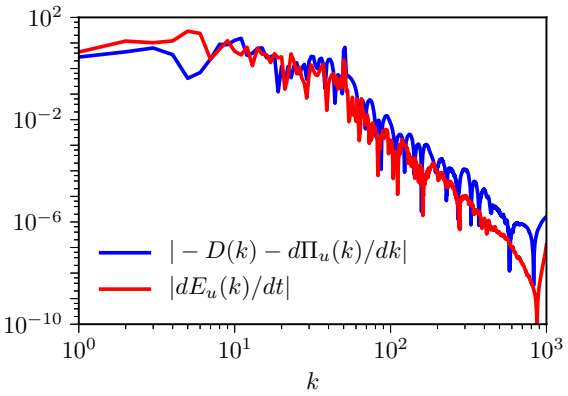


FIG. 4. For 2D simulation on the $2048^2$ grid, plots of $|-D(k)-d\Pi_u(k)/dk|$ and $|\partial E(k,t)/\partial t|$. Significant measures of $|\partial E(k,t)/\partial t|$ indicate the unsteady nature of the flow.

noticeably, $|\partial E(k)/\partial t|$ is significant for $k < k_f$. Note, however, that these quantities are small for $k > k_f$. This is the reason for the unsteady nature of the flow that leads to strong fluctuations in $\Pi_u(k)$ and $\Pi_\omega(k)$ in the $k < k_f$ regime.

In the next subsection, we describe the shell-to-shell energy transfers for 2D turbulence.

### C. Shell-to-shell energy transfers

In the present subsection we describe the shell-to-shell energy transfers for 2D turbulence. We compare our results with those from three-dimensional turbulence for which the shell-to-shell transfers are local and forward [56,57].

We compute the shell-to-shell energy transfers in the wavenumber band $k < k_f$ using the formula of Eq. (41). As described in Sec. IV, for the $8192^2$ grid simulation we divide this wavenumber region into 20 shells. The computed energy transfers are exhibited in Fig. 5.

In Fig. 5(a), we plot the shell-to-shell energy transfers $T^{u,m}_{u,n}$ vs $n-m$ computed for a single frame. Here $m$ and $n$ are the giver and receiver shells, respectively. These transfers exhibit significant fluctuations for different data sets; hence we average the transfer rates for 35 frames. The averaged transfers are exhibited in Fig. 5(b). As shown in the figures, especially Fig. 5(b), shell $n$ receives energy from shell $n-1$ and gives energy to shell $n+1$. Hence, among the nearest-neighbor shells in the inertial range of $k < k_f$, the energy transfer in 2D hydrodynamic turbulence is forward. Note, however, that $T^{u,m}_{u,n} < 0$ when $n-m > 2$ or 3 (for some shells). This implies that small wavenumbers receive energy from distant but larger wavenumbers. Therefore, in 2D hydrodynamic turbulence, the shell-to-shell energy transfers to the neighboring shells are forward, but they are backward for the distant shells.

In Figs. 5(c) and 5(d), we exhibit the corresponding density plots. Here, the indices of the $x$ and $y$ axes represent the receiver and giver shells, respectively. Though the plots exhibit significant fluctuations, the density plots are consistent with the results of Figs. 5(a) and 5(b).

The aforementioned shell-to-shell energy transfers of 2D turbulence differ significantly from the those of 3D turbulence for which the transfers are local and forward for the inertial

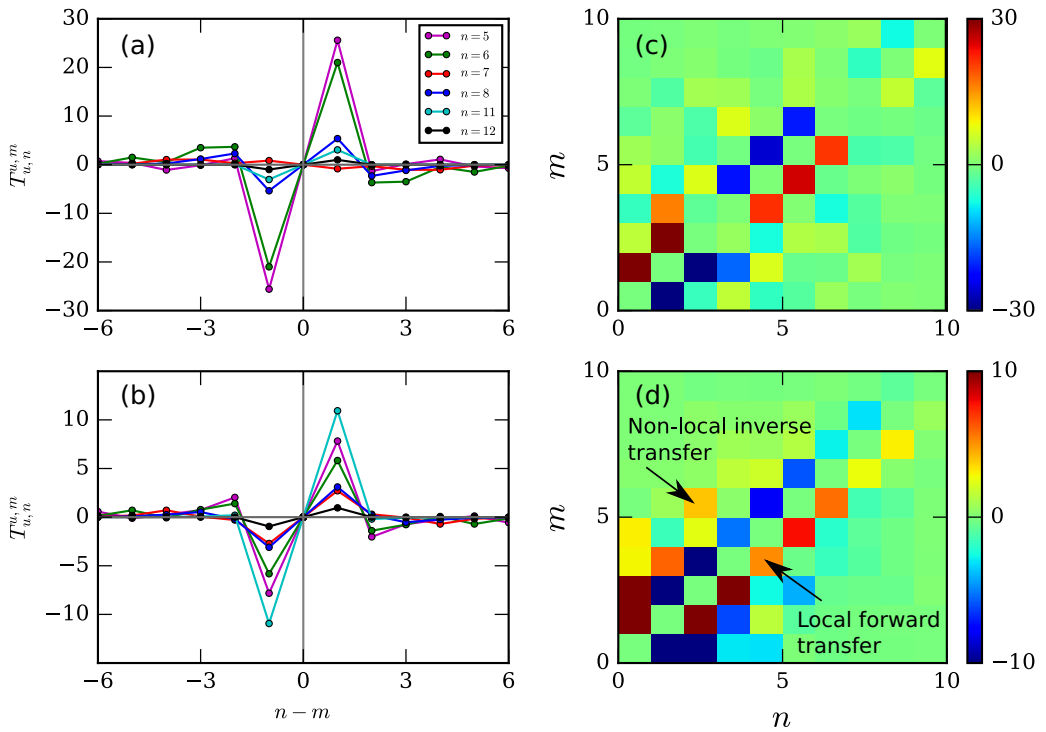


FIG. 5. For 2D simulation on the $8192^2$ grid, plots of the shell-to-shell energy transfers $T^{u,m}_{u,n}$ vs $n-m$ in the inertial range of the $k < k_f$ regime (a) for a single time frame, (b) for time-averaged data with 35 frames, and (c, d) density plots of shell-to-shell energy transfers $T^{u,m}_{u,n}$ corresponding to (a) and (b), respectively. The $x$ and $y$ axes represent the receiver and giver shells, respectively. The energy transfers are local and forward for neighboring shells, but nonlocal and backward for distant shells.

range shells. This divergence between the 2D and 3D flows is due to the inverse cascade of energy. Verma *et al.* [57] computed the shell-to-shell energy transfers for 2D turbulence using field-theoretic tools and reported local forward and nonlocal backward energy transfers for $k < k_f$ (consistent with the aforementioned numerical simulations); they showed that these complex transfers add up to yield a negative $\Pi_u(k)$. Here, the nonlocal backward energy transfers from many shells play a critical role.

We summarize our results in the next section.

## VI. CONCLUSIONS

In this paper we present several results on 2D forced turbulence with forcing employed at intermediate scales. Using Pao's conjecture, we extend Kraichnan's [22] power-law predictions for 2D turbulence beyond the inertial range. In the new scaling solution, the power laws are coupled with exponential functions of $k$.

To test the model predictions, we performed numerical solution of 2D turbulence on $2048^2$ and $8192^2$ grids with forcing at (50,51) and (100,101) wavenumber bands, respectively. We computed the spectra and fluxes of energy and enstrophy using the numerical data, and compared them with the model predictions. We observe that the model predictions and numerical results on the energy and enstrophy spectra and fluxes agree with each other for $k > k_f$. In this regime, the energy spectrum is steeper than $k^{-3}$, which is primarily due to the exponential factor $\exp(-(k/k_{d2D})^2)$ of Eq. (32). The situation, however, is different for $k < k_f$. Though the energy spectrum follows a $k^{-5/3}$ power law, the energy and enstrophy fluxes exhibit significant fluctuations that arise possibly due to the unsteady nature of the flow. The fluctuations are somewhat suppressed on averaging. These issues need further investigation.

We also compute the shell-to-shell energy transfers in the $k < k_f$ regime. We observe forward energy transfers for the nearest-neighbor shells, but backward energy transfers for the other shells, consistent with the analytical findings of Verma *et al.* [57]. The nonlocal backward transfers add up to yield a negative energy flux. In addition, we observe that the shell-to-shell energy transfers in the $k < k_f$ regime exhibit significant fluctuations among different frames due to the unsteady nature of the flow.

We also remark that rapidly rotating turbulence, and magnetohydrodynamic and quasistatic magnetohydrodynamic turbulence with strong external magnetic field, exhibit quasi-2D behavior [12–18]. Sharma *et al.* [14] employed the enstrophy flux derived in Sec. III to describe the energy spectra and flux of rapidly rotating turbulence. Similar attempts have been made to explain the turbulence properties of quasistatic magnetohydrodynamic turbulence [15–18]. In addition, two-dimensional magnetohydrodynamic turbulence too exhibits interesting properties (e.g., see Ref. [58]), but these discussions are beyond the scope of this paper.

In summary, our findings on 2D turbulence shed interesting light on the energy and enstrophy transfers. In the future, we plan to extend the present work to the regime of constant enstrophy flux. In particular, we hope to study the shell-to-shell enstrophy transfers and explore whether they are local or nonlocal. In addition, it will be interesting to extend the models discussed in Sec. III in the presence of Ekman friction.

## ACKNOWLEDGMENTS

We thank Manohar Sharma for useful discussions and Shaswant Bhattacharya for comments on the manuscript. Our numerical simulations were performed on Shaheen II at the Kaust supercomputing laboratory, Saudi Arabia, under the project k1052. This work was supported by Research Grant No. PLANEX/PHY/2015239 from the Indian Space Research Organisation, India; by the Indo-Russian project INT/RUS/RSF/P-03 from the Department of Science and Technology, India; and by the IITK institute postdoctoral fellowship to A.G.

[1] W. D. McComb, *The Physics of Fluid Turbulence* (Clarendon Press, Oxford, 1990).
[2] U. Frisch, *Turbulence: The Legacy of A. N. Kolmogorov* (Cambridge University Press, Cambridge, UK, 1995).
[3] *The Theory of Turbulence: Subrahmanyan Chandrasekhar's 1954 Lectures*, edited by E. A. Spiegel (Springer, Berlin, 2010).
[4] M. Lesieur, *Turbulence in Fluids* (Springer-Verlag, Dordrecht, 2008).
[5] A. Alexakis and L. Biferale, Phys. Rep. **767–769**, 1 (2018).
[6] Y. B. Kolesnikov and A. B. Tsinober, Fluid Dyn. **9**, 621 (1976).
[7] H. Kellay and W. I. Goldburg, Rep. Prog. Phys. **65**, 845 (2002).
[8] P. Tabeling, Phys. Rep. **362**, 1 (2002).
[9] H. J. H. Clercx and G. J. F. van Heijst, Appl. Mech. Rev. **62**, 020802 (2009).
[10] M. K. Verma, Europhys. Lett. **98**, 14003 (2012).
[11] G. Boffetta and R. E. Ecke, Annu. Rev. Fluid Mech. **44**, 427 (2012).
[12] D. Oks, P. D. Mininni, R. Marino, and A. Pouquet, Phys. Fluids **29**, 111109 (2017).
[13] H. Xia and N. Francois, Phys. Fluids **29**, 111107 (2017).
[14] M. K. Sharma, A. Kumar, M. K. Verma, and S. Chakraborty, Phys. Fluids **30**, 045103 (2018).
[15] A. Pothérat, J. Sommeria, and R. Moreau, J. Fluid Mech. **424**, 75 (2000).
[16] H. Lee, D. Ryu, J. Kim, T. W. Jones, D. Balsara, and D. S. Balsara, Astrophys. J. Lett. **594**, 627 (2003).
[17] K. S. Reddy and M. K. Verma, Phys. Fluids **26**, 025109 (2014).
[18] M. K. Verma, Rep. Prog. Phys. **80**, 087001 (2017).
[19] E. Lindborg and A. Vallgren, Phys. Fluids **22**, 091704 (2010).
[20] P. A. Davidson, *Turbulence in Rotating, Stratified and Electrically Conducting Fluids* (Cambridge University Press, Cambridge, UK, 2013).
[21] M. K. Verma, *Physics of Buoyant Flows: From Instabilities to Turbulence* (World Scientific, Singapore, 2018).
[22] R. H. Kraichnan, Phys. Fluids **10**, 1417 (1967).
[23] J. Paret and P. Tabeling, Phys. Rev. Lett. **79**, 4162 (1997).
[24] T. Gotoh, Phys. Rev. E **57**, 2984 (1998).

[25] M. K. Nandy and J. K. Bhattacharjee, Int. J. Mod. Phys. B **09**, 1081 (1995).
[26] R. H. Kraichnan, J. Fluid Mech. **47**, 525 (1971).
[27] M. A. Rutgers, Phys. Rev. Lett. **81**, 2244 (1998).
[28] Y.-L. Xiong, C.-H. Bruneau, and H. Kellay, Europhys. Lett. **95**, 64003 (2011).
[29] E. D. Siggia and H. Aref, Phys. Fluids **24**, 171 (1981).
[30] U. Frisch, Phys. Fluids **27**, 1921 (1984).
[31] V. Borue, Phys. Rev. Lett. **72**, 1475 (1994).
[32] L. M. Smith and V. Yakhot, Phys. Rev. Lett. **71**, 352 (1993).
[33] B. Legras, P. Santangelo, and R. Benzi, Europhys. Lett. **5**, 37 (1988).
[34] H. Kellay, X-l. Wu, and W. I. Goldburg, Phys. Rev. Lett. **74**, 3975 (1995).
[35] R. K. Scott, Phys. Rev. E **75**, 046301 (2007).
[36] J. Fontane, D. G. Dritschel, and R. K. Scott, Phys. Fluids **25**, 015101 (2013).
[37] R. Pandit, D. Banerjee, A. Bhatnagar, M. E. Brachet, A. Gupta, D. Mitra, N. Pal, P. Perlekar, S. S. Ray, V. Shukla, and D. Vincenzi, Phys. Fluids **29**, 111112 (2017).
[38] M. Eghdami, S. Bhushan, and A. P. Barros, J. Atmos. Sci. **75**, 1163 (2018).
[39] G. Boffetta, J. Fluid Mech. **589**, 253 (2007).
[40] S. Danilov and D. Gurarie, Phys. Rev. E **63**, 061208 (2001).
[41] S. Musacchio and G. Boffetta, Phys. Rev. Fluids **4**, 022602 (2019).
[42] A. N. Kolmogorov, Dokl. Akad. Nauk SSSR **30**, 301 (1941).
[43] A. N. Kolmogorov, Dokl. Akad. Nauk SSSR **32**, 16 (1941).
[44] Y.-H. Pao, Phys. Fluids **8**, 1063 (1965).
[45] Y.-H. Pao, Phys. Fluids **11**, 1371 (1968).
[46] S. B. Pope, *Turbulent Flows* (Cambridge University Press, Cambridge, UK, 2000).
[47] D. O. Martínez, S. Chen, G. D. Doolen, R. H. Kraichnan, L.-P. Wang, and Y. Zhou, J. Plasma Phys. **57**, 195 (1997).
[48] M. K. Verma, A. Kumar, P. Kumar, S. Barman, A. G. Chatterjee, R. Samtaney, and R. Stepanov, Fluid Dyn. **53**, 728 (2018).
[49] M. Abramowitz and I. A. Stegun, *Handbook of Mathematical Functions, with Formulas, Graphs, and Mathematical Tables* (Dover Publication, Inc., New York, 1965).
[50] M. K. Verma, A. G. Chatterjee, R. K. Yadav, S. Paul, M. Chandra, and R. Samtaney, Pramana **81**, 617 (2013).
[51] A. G. Chatterjee, M. K. Verma, A. Kumar, R. Samtaney, B. Hadri, and R. Khurram, J. Parallel Distrib. Comput. **113**, 77 (2018).
[52] C. Canuto, M. Y. Hussaini, A. Quarteroni, and T. A. Zang, *Spectral Methods in Fluid Dynamics* (Springer-Verlag, Berlin, 1988).
[53] J. P. Boyd, *Chebyshev and Fourier Spectral Methods*, 2nd ed. (Dover Publications, New York, 2003).
[54] G. Dar, M. K. Verma, and V. Eswaran, Physica D **157**, 207 (2001).
[55] M. K. Verma, Phys. Rep. **401**, 229 (2004).
[56] J. A. Domaradzki and R. S. Rogallo, Phys. Fluids A **2**, 414 (1990).
[57] M. K. Verma, A. Ayyer, O. Debliquy, S. Kumar, and A. V. Chandra, Pramana **65**, 297 (2005).
[58] P. D. Mininni, D. C. Montgomery, and A. G. Pouquet, Phys. Fluids **17**, 035112 (2005).